Multimodal Odometry Estimation With Automated Sensor Selection

Martin Michaelis, Philipp Berthold, Thorsten Luettel and Mirko Maehlisch

***Abstract*—For autonomous driving applications, knowledge of the ego position, orientation, and velocity is a necessary prerequisite for recognizing landmarks and moving targets. We use radar sensors for the determination of these quantities in a radar odometry system. Radar odometry uses the advantage of a direct measurement of the radial speed using radar sensors. Radar sensors are less susceptible to bad weather and lighting conditions than camera and lidar sensors. In addition, radar data is not susceptible to wheel slippage or blocked wheels compared with wheel speed measurements. However, radar data is still susceptible to clutter. In order to achieve a combination of good precision under optimal conditions and good precision under adverse weather conditions, we fuse measurements from radar sensors, wheel speed sensors and the gyrometer. We do not simply combine these measurements according to assumed covariances. Instead, we check the plausibility of the measurements based on their likelihood. Subsequently, we weight the results of the sensor combinations accordingly. The decision about sensor weighting is carried out in a principled, probabilistic manner and adaptively with regard to environmental influences. We validate our approach using real data. Our approach is more precise under adverse conditions than using wheel speed sensors and gyrometers alone. On the other hand, it is more precise under good conditions than using only radar measurements.**

I. Introduction

Radar has emerged as a promising sensor in autonomous driving. One factor is that radar sensors are cost efficient. Another factor is the relative precision of radar sensors under bad weather conditions in comparison with other external sensors like lidar and camera sensors. Radar sensors are independent of lighting conditions, which play a big role for cameras. Even lidar sensors are prone to errors in low sun settings. In addition to being more robust with respect to weather conditions, radar offers the advantage of a direct radial speed measurement. This radial speed measurement is still in its early stages in lidar sensors and not available for camera sensors.

It is the radial speed measurement that we exploit in order to estimate the ego velocity. As soon as we identify static points and observe multiple static points in different directions, we can estimate our ego velocity. The ego velocity is then integrated in a dead reckoning approach to estimate the ego position. As it is crucial to use only static object measurements, we have dedicated some attention to this part. In a previous work [1], we have shown that it is more precise to use expected measurements in order to identify static object measurements, compared with the random sample consensus (RANSAC) approach. In this work, we provide further comparison of the different mechanisms to identify static points. In addition, we compare the radar odometry with the classical odometry solution that combines wheel speed measurements and gyrometer measurements. The wheel speed measurements indicate the speed at which the wheels turn. The gyrometer measurements indicate the speed at which the orientation changes. Under adverse conditions, in our case snowy roads, the radar odometry performs better than the classical odometry solution.

All authors are with the Institute for Autonomous Systems Technology (TAS) of the University of the Bundeswehr Munich, Neubiberg, Germany. Contact author email: {martin.michaelis, tas}@unibw.de

Fig. 1. Test vehicle under adverse weather conditions.

Even with our refined static object selection for the radar odometry, the classical combination of wheel speed measurements and gyrometer measurements tends to be more accurate under good weather conditions. In order to benefit from the precision of the classical odometry under good conditions, as well as being able to use the relatively good precision of radar measurements under adverse conditions, we develop an approach that combines both sensor sets. We want to use this system without manual intervention, i.e., without manual selection of the sensor setup according to the road conditions. If we fused the measurements from both systems directly, wheel speed measurements would still have a bigger impact, thus the fused estimate would still suffer under adverse conditions. Instead, we determine which system to use in a probabilistic manner. To this end, we use expected measurements. The likelihood of actual measurements given the expected ones is used to determine the validity of each sensors' readings. Then, the estimates based on each sensor are weighted accordingly. Formally, this relies on the same reasoning as the interacting multiple model (IMM) filter, which chooses motion models probabilistically.

Our contribution is a fusion of radar measurements, wheel

speed measurements and gyrometer measurements in a principled, probabilistic manner. We evaluate the validity of our approach using real data from our autonomous test vehicle. Our results achieve a combination of good precision under adverse conditions and good precision under good conditions. The precision of the fused results surpasses the classical odometry and the radar odometry both under good and adverse weather conditions.

The rest of the paper is structured as follows: We formulate the radar odometry problem and the odometry fusion problem in Sec. II. Sec. III presents related works. We develop our contribution in Sec. IV. In Sec. V, we evaluate our fused results and compare them to the solutions based on individual sensing modalities. Finally, Sec. VI concludes the paper and Sec. VII proposes future work.

II. Problem Formulation

The radar odometry and dead reckoning problem is to estimate the ego vehicle state using radar data. We define the state as

$$\mathbf{x} = (x \; y \; \varphi \; v \; \omega)^\top, \tag{1}$$

where x and y are the two-dimensional position of the ego, φ is its yaw angle, v is the one-dimensional vehicle speed and ω is the yaw rate. The speed v and the yaw rate ω are estimated first. Then, assuming an initial position and yaw of zero, subsequent poses can be obtained using the constant turn rate and velocity (CTRV) model

$$f(\mathbf{x}, \Delta t) = \begin{pmatrix} x + \frac{v}{\omega}(-\sin(\varphi) + \sin(\varphi + \omega\,\Delta t)) \\ y + \frac{v}{\omega}(\cos(\varphi) - \cos(\varphi + \omega\,\Delta t)) \\ \varphi + \omega\,\Delta t \\ v \\ \omega \end{pmatrix}. \tag{2}$$

A special case of this is the limiting case with $\omega \approx 0$, which results in the constant velocity model

$$f(\mathbf{x}, \Delta t) = \begin{pmatrix} x + \cos(\varphi)\, v\, \Delta t \\ y + \sin(\varphi)\, v\, \Delta t \\ \varphi \\ v \\ 0 \end{pmatrix}. \tag{3}$$

From all measurements at time step k in $\mathcal{Y}^k$, we need to determine a subset $\bar{\mathcal{Y}}^k \subset \mathcal{Y}^k$ of static object measurements.

The measurement in polar coordinates consists of the measured distance y_r and the measured angle y_β. In addition, the measurement of the Doppler velocity y_v is given as the derivative of the measured distance y_r as

$$y_v = \dot{y_r}. \tag{4}$$

The measured polar coordinates can be converted to the measured Cartesian coordinates y_x and y_y.

With different sensor modalities, we obtain different estimates for the speed and yaw rate, and consequently also for the position and yaw. The multi-modal selection problem is defined as combining the estimates in a probabilistic manner where the state $\mathbf{x}_k$ at time step k is represented as a Gaussian mixture with l components as

$$p(\mathbf{x}_k|\mathcal{Y}_{1:k}) = \sum_{i_k} p_{i_k}\, p(\mathbf{x}_{i_k}|\mathcal{Y}_{1:k}), \tag{5}$$

where p_{i_k} is the probability of the i_k-th mode and $\mathbf{x}_{i_k}$ is the state conditioned on the i_k-th mode.

III. Related Work

An overview over radar odometry solutions is given in [2]. There, it is also stated that there is a relative lack of sensor fusion for odometry purposes. Examples for the fusion of radar and camera data are [3] and [4]. Inertial data is fused with radar in [5]–[8], which performs a time trajectory optimization. Radar is also fused with classical odometry sensors like wheel speed sensors and a gyrometer in [9]. A diverse sensor setup with inertial data, global navigation satellite system, lidar and radar sensors is used in [10].

As we look into radar odometry solutions in more detail, we distinguish Doppler-based methods, matching-based methods or learning-based methods. Doppler-based methods are [1], [11]–[14]. The first three use expected measurements for the outlier and static object detection. The bearing uncertainty of radar measurements is incorporated in [15].

Next, we look into matching-based approaches which match either features or whole radar scans. Examples for these approaches are [16]–[23].

Combinations of direct Doppler-based approaches and matching are presented in [24]–[26].

An unsupervised learning approach is presented in [27]. This paper also presents a good overview over other learning-based methods.

Our rationale for using a Doppler-based algorithm rather than a matching-based one, is that the comparison of radar data from different time steps is not easy due to the fluctuating nature of radar measurements [7]. This task becomes easier with higher resolution imaging radar data, which is not available in our case. Learning-based algorithms incur higher computational costs, and introduce latency which is suboptimal in odometry applications, as the odometry estimate is a prerequisite for further calculation steps.

IV. Algorithm

In this section we will present our approach in four parts. First, we give a brief review of the radar-based odometry estimation. Second, we describe how to use this approach in conjunction with wheel speed measurements and with gyrometer measurements. Third, we discuss the selection of static points, on which the calculations are based. Finally, we discuss the automatic model selection from these possibilities.

A. Radar-based odometry estimation

We start with a brief review of Doppler velocity measurements. More details of the derivation can be found in [1], [13], [28], [29]. Since we want to determine the ego position in the first place, we cannot use it to convert the measurements to

world coordinates. Consequently, we use the measurements in ego coordinates.

The perceived velocity is the difference between the velocity of the detected point $\mathbf{v}_D$ and the perceived sensor velocity $\mathbf{v}_S$. Then, the perceived radial speed is the radial component of the perceived velocity. The measurement angle β is defined as the angle between the line from the sensor to the measurement and the vehicle heading, the projection is performed using the scalar product:

$$y_v = \begin{pmatrix}\cos(\beta) & \sin(\beta)\end{pmatrix} (\mathbf{v}_D - \mathbf{v}_S) \,. \tag{6}$$

A static object measurements implies that $\mathbf{v}_D = 0$, which results in the simplified equation

$$y_v = - \begin{pmatrix}\cos(\beta) & \sin(\beta)\end{pmatrix} \mathbf{v}_S. \tag{7}$$

Here, the sensor velocity in ego coordinates is given by

$$\mathbf{v}_S = \begin{pmatrix} v - \omega\, y_S \\ \omega\, x_S \end{pmatrix}, \tag{8}$$

where $(x_S \;\; y_S)^\intercal$ is the sensor location in ego coordinates. Using (8) in (7) gives us

$$y_v = -v\cos(\beta) + \cos(\beta)\,\omega\, y_S - \sin(\beta)\,\omega\, x_S. \tag{9}$$

In (9), y_v and β are measured quantities, and the mounting positions x_S and y_S are constants. Thus, the only unknowns are v and ω. With at least two suitable radial velocity measurements, we can determine the unknowns from (9). To this end, we use a least squares algorithm with Householder transformations. In order for this to be possible, we need to have measurements from at least two different angles β.

B. Static Point Selection

We have made the assumption of static objects in (7). If we were to use all radar measurements in the odometry calculation, the assumption that $\mathbf{v}_D = 0$ would be violated and thus lead to incorrect results. We use prior knowledge to determine the subset of static object measurements $\bar{\mathcal{Y}}^k \subset \mathcal{Y}^k$, i.e., to determine which measurements can be used in the odometry calculation. For high measurement update rates the speed and yaw rate of the ego vehicle do not change much between subsequent measurement cycles. The time interval between subsequent radar measurements is $50\,\mathrm{ms}$ or lower in our application. Substituting the previous ego speed estimate $\hat{v}_{k-1}$ and previous yaw rate $\hat{\omega}_{k-1}$ in (9), we obtain

$$y_v^\star = -\hat{v}_{k-1}\cos(\beta) + \cos(\beta)\,\hat{\omega}_{k-1}\, y_S - \sin(\beta)\,\hat{\omega}_{k-1}\, x_S. \tag{10}$$

If the difference is below a threshold, the measurement is considered to be a static object measurement and included in $\bar{\mathcal{Y}}^k$. The threshold consists of one term that accounts for the error between time steps, where the expected error in the velocity is the product of the maximum acceleration $a_{\max}$ and the time since the last measurement Δt_k. This expected radial velocity is compared to the measured radial velocity:

$$|y_v^\star - y_v| < a_{\max}\Delta t_k + 2\sigma_v, \tag{11}$$

where σ_v is the standard deviation of the radial velocity measurement. The maximum time interval is $50\,\mathrm{ms}$. The maximum acceleration can be assumed as $a_{\max} \approx 1\mathrm{g} = 9.81\,\mathrm{m/s^2}$. This bound needs to account for the effect of a changing yaw rate, too. Thus, we use a bound of $1.0\,\mathrm{m/s}$. With the static object measurements we obtain $\hat{v}_k$ and $\hat{\omega}_k$.

As mentioned, all previous calculations were necessarily performed in ego coordinates. Since speed and yaw rate are the same in global coordinates, we can use them in the global reference frame in the integration of position and yaw estimates with (2).

Initially, we have $\hat{x}_0 = \hat{y}_0 = 0.0\,\mathrm{m}$ and $\hat{\varphi}_0 = 0.0°$. Often, the vehicle is initially standing. Then, $\hat{v}_0 = 0\,\mathrm{m/s}$ and $\hat{\omega}_0 = 0\,°/\mathrm{s}$. If this assumption does not hold, we can still select a first set of static object measurements using the RANSAC algorithm.

C. Combination with Wheel Speed or Gyrometer Measurements

In order to combine the radar measurements with wheel speed sensors or gyrometers, we substitute the measured quantities in (9). With the measured velocity $\bar{v}$ from wheel speed measurements, we obtain the modified measurement equation

$$y_v = -\bar{v}\cos(\beta) + \cos(\beta)\,\omega\, y_S - \sin(\beta)\,\omega\, x_S. \tag{12}$$

Similarly, with the yaw rate $\bar{\omega}$ from the gyrometer measurement, we obtain

$$y_v = -v\cos(\beta) + \cos(\beta)\,\bar{\omega}\, y_S - \sin(\beta)\,\bar{\omega}\, x_S. \tag{13}$$

These two possibilities can each be used in order to replace (9), where it is then only necessary to solve the measurement equations for one variable.

D. Automated Modality Selection

We have four possibilities to obtain odometry measurements, as summarized in Tab. I. These result from suitable combinations of the radar sensors, wheel speed sensors, and the gyrometer. The first possibility is to use solely radar measurements, as described in Sec. IV-A. The second and third possibility is to combine radar measurements either with measurements from wheel speed sensors, or from the gyrometer, as described in Sec. IV-C. The fourth possibility is not to use radar measurements at all, as in classical odometry applications. We will call these possibilities measurement modes. We will automatically select which of these measurement modes to use, based on the measurement likelihoods and a process which describes that the optimal measurement mode is likely to stay the same between subsequent time steps. To

TABLE I
MEASUREMENT MODALITY COMBINATIONS

Modality	***Radar***	***Wheel speed***
Radar	1	3
Gyrometer	2	4

this end, we adapt the methodology of the interacting multiple model filter to our case.

The state $\mathbf{x}_k$ at time step k is represented as a Gaussian mixture with l components as

$$p(\mathbf{x}_k|\mathcal{Y}_{1:k}) = \sum_{i_k} p_{i_k}\, p(\mathbf{x}_{i_k}|\mathcal{Y}_{1:k}), \tag{14}$$

where p_{i_k} is the probability of the i_k-th mode and $\mathbf{x}_{i_k}$ is the state conditioned on the i_k-th mode. Then, the mode probability p_{i_k} for the ith mode at time step k is given as

$$\begin{aligned} p_{i_k} &\propto p(\mathbf{y}_k|\mathbf{y}_{1:k-1})\, p(i_k|\mathbf{y}_{1:k-1}) && (15)\\ &= p(\mathbf{y}_k|\mathbf{y}_{1:k-1}) \sum_{i_{k-1}} p(i_k|i_{k-1})\, p(i_{k-1}|\mathbf{y}_{1:k-1}) && (16)\\ &= p(\mathbf{y}_k|\mathbf{y}^\star_{i_k}) \sum_{i_{k-1}} \mu_{i_{k-1}i_k} p_{i_{k-1}}, && (17) \end{aligned}$$

where $\mu_{i_{k-1}i_k}$ is the probability of the mode i_k following mode i_{k-1}. In our application we use $\mu_{i_{k-1}i_k} = 0.99$ if $i_k = i_{k-1}$ and split the remaining probability equally between all other mode transitions. This gives us a recursion for the mode probabilities that uses the measurement likelihood with respect to the expected likelihood.

The idea is to use this approach, although we do not really use different motion models. However, we can transport this idea to our situation. In order to do so, we pretend that velocities and yaw rates of the different measurement modes are different quantities. Then, we define different motion models that really differ only in which velocity and yaw rate they use in the computation of the position and yaw. To this end, we define a stacked state which consists one pair of speed and yaw rate for each measurement modality

$$\mathbf{x} = (x\ y\ \varphi\ v_1\ \omega_1 \cdots v_l\ \omega_l)^\top \tag{18}$$

where we assume l different measurement modalities. With this stacked state, we can define stacked motion models, where each model corresponds to one measurement modality. Then, the position and yaw depend on the velocity and yaw rate of the respective measurement modes:

$$f_i(\mathbf{x}) = \begin{pmatrix} x + \frac{v_i}{\omega_i}(-\sin(\varphi) + \sin(\varphi + \omega_i\,\Delta t)) \\ y + \frac{v_i}{\omega_i}(\cos(\varphi) - \cos(\varphi + \omega_i\,\Delta t)) \\ \varphi + \omega_i\,\Delta t \\ v_1 \\ \omega_1 \\ \vdots \\ v_l \\ \omega_l \end{pmatrix}. \tag{19}$$

In our special case, some of the speed and yaw rate values are the same, however we keep them as separate values in the notation in order to preserve generality and notational simplicity.

V. Evaluation

A. Algorithms

1) Radar RANSAC algorithm: This algorithm uses the RANSAC algorithm in the determination of static object measurements, as it is quite common in the literature. It has been used in [1] as the baseline. In each iteration, we draw two random measurements. We determine speed and yaw rate estimates with (9). These speed and yaw rate estimates are used in (10) such that we obtain an expected measurement corresponding to each actual measurement. With (11), we determine whether expected and actual measurement fit the static object hypothesis.

After a set number of iterations (100 in our case), we select the hypothesis with the most conforming measurements. The conforming measurements are used in (11) for the final speed and yaw rate estimates. We integrate the dead reckoning solution using (2).

2) Radar algorithm: The radar odometry solution with a static object detection-based on expected measurements as developed in [1], which was reviewed briefly in Sec. IV-A and Sec. IV-B, is used.

3) Classical algorithm: In a classical approach, the mean wheel speed readings are used as an estimate for the velocity, and the gyrometer reading is used as an estimate for the yaw rate. These estimates are integrated using dead reckoning to obtain position and yaw estimates.

4) Fused algorithm: The radar and the classical algorithm and their components are fused as described in Sec. IV-D.

B. Scenarios

We evaluate the algorithms in three real data experiments. The ego vehicle is equipped with six radars. Four short range radars are located at the corners of the vehicle, and one more is located at the center of the front. In addition, one far range radar is located at the center of the front. This setup provides all-round coverage. The ego vehicle is equipped with a RTK-GNSS-based inertial navigation system (INS) for reference purposes. In the first scenario, two targets equipped with RTK-GNSS INS are present. The static object detection used in the algorithms does of course not use the data from the reference system. The basic facts for the three scenarios are displayed in Tab. II.

TABLE II
Scenario desription

Scenario	*Starting speed*	*Ending speed*	*Road*	*Targets*
1	$9\,\mathrm{m/s}$	$8\,\mathrm{m/s}$	Good	2
2	$0\,\mathrm{m/s}$	$8\,\mathrm{m/s}$	Snow	0
3	$7\,\mathrm{m/s}$	$0\,\mathrm{m/s}$	Snow	0

1) Scenario 1: This scenario takes place under good road conditions. The ego vehicle follows two target vehicles on a curvy road as displayed in Fig. 2. The scenario covers a trajectory length of $222\,\mathrm{m}$ over a duration of $25\,\mathrm{s}$. It starts with moving vehicles, which drive at a constant speed of approximately $9\,\mathrm{m/s}$.

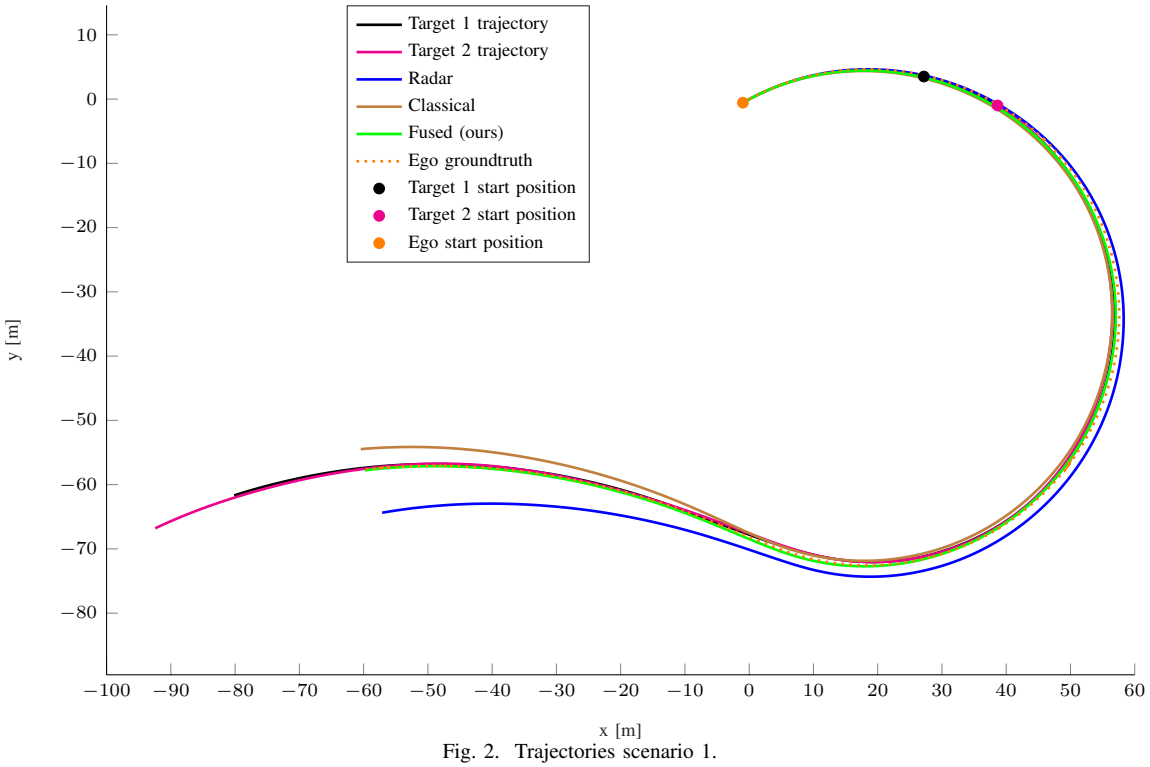

Fig. 2. Trajectories scenario 1.

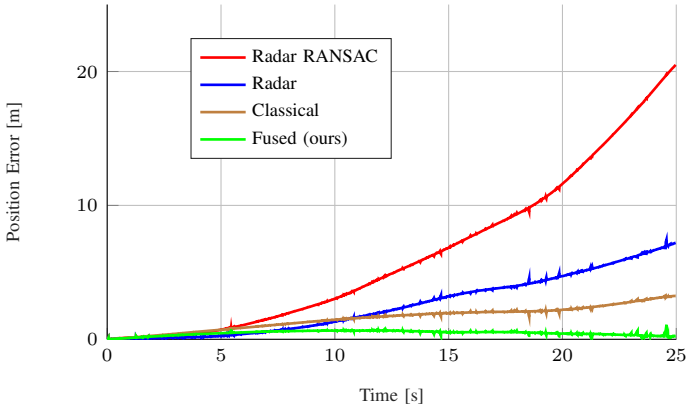

Fig. 3. Position error scenario 1.

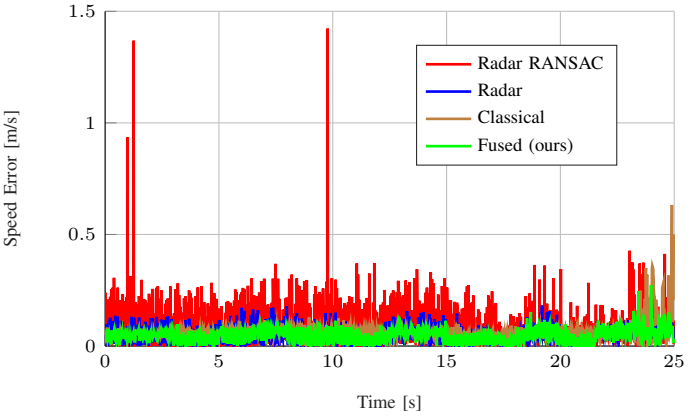

Fig. 5. Speed error scenario 1.

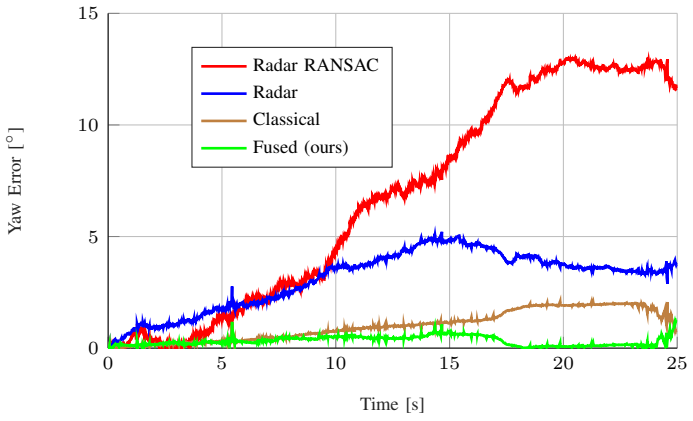

Fig. 4. Yaw error scenario 1.

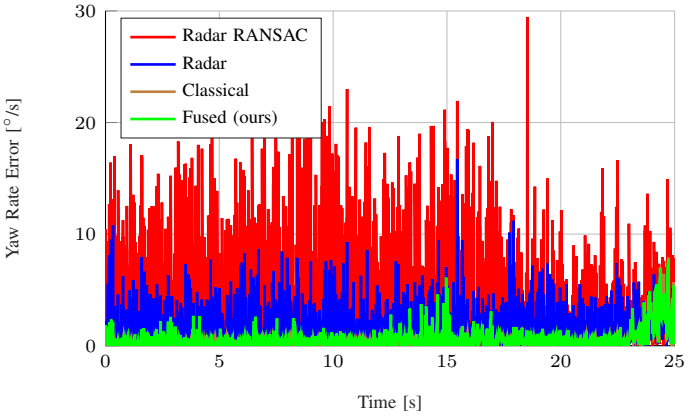

Fig. 6. Yaw rate error scenario 1.

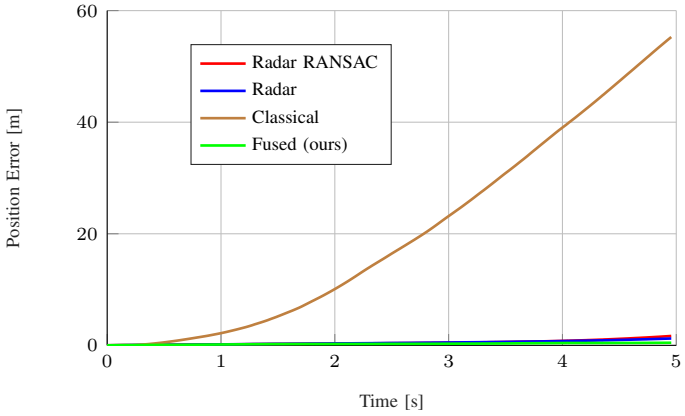

Fig. 7. Position error scenario 2.

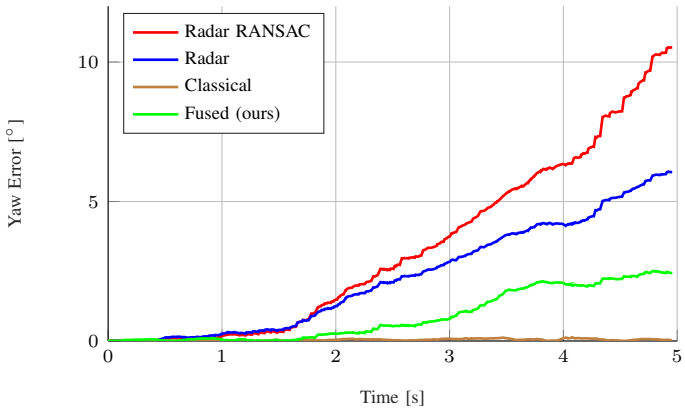

Fig. 8. Yaw error scenario 2.

2) Scenario 2: This scenario takes place on flattened snow. The ego vehicle accelerates to $8\,\mathrm{m/s}$ during $5\,\mathrm{s}$. During the scenario, it covers $20\,\mathrm{m}$ on a rather straight line.

3) Scenario 3: This scenario also takes place on flattened snow. The ego vehicle initially moves with $7\,\mathrm{m/s}$ and brakes to a stand still in $5\,\mathrm{s}$. During this scenario, it covers $17\,\mathrm{m}$ on a straight line.

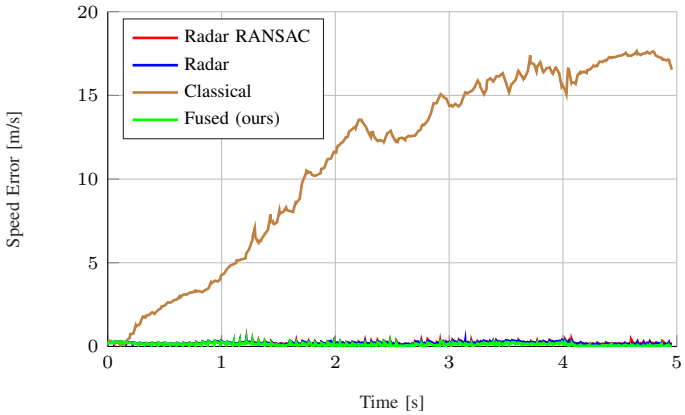

Fig. 9. Speed error scenario 2.

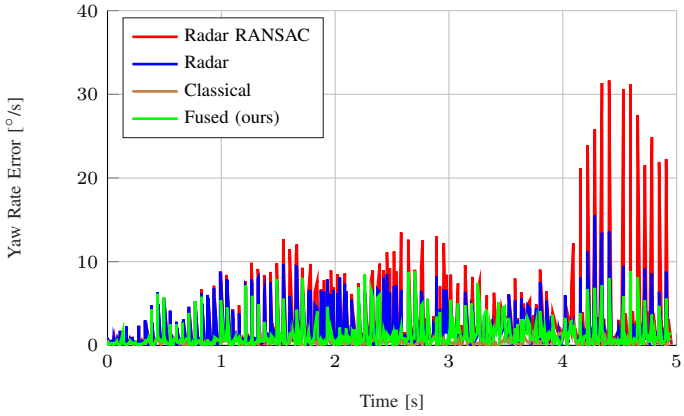

Fig. 10. Yaw rate error scenario 2.

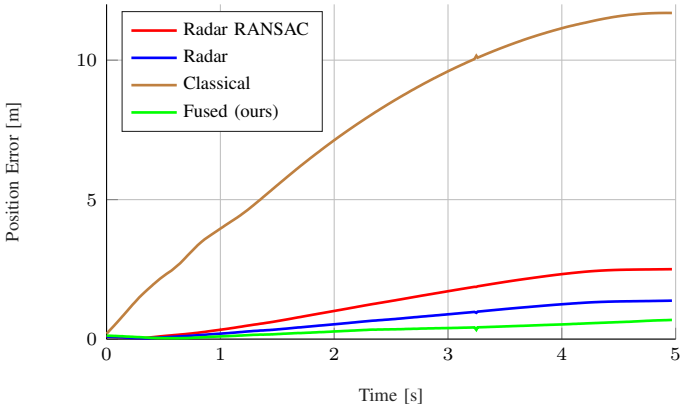

Fig. 11. Position error scenario 3.

C. Results

1) Scenario 1: The accuracy of the algorithms is shown in Fig. 3 - Fig. 6. Mean errors are summarized in Tab. III. The estimated trajectories are compared to the real trajectory in Fig. 2. Overall, the fused algorithm matches the better speed accuracy of the radar odometry and the better yaw rate accuracy of the classical algorithm. As a result, it outperforms both of these algorithms in the accuracy of the integrated position

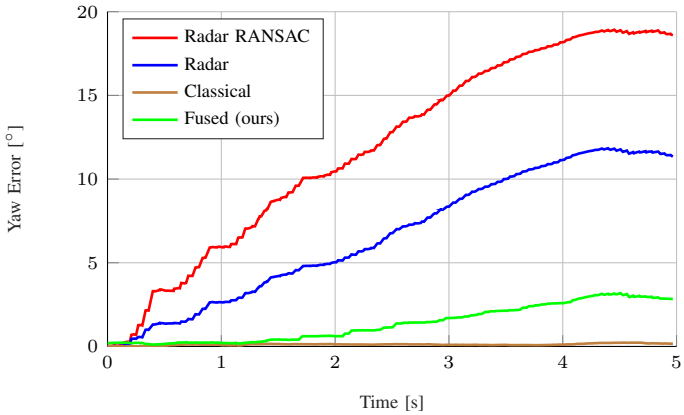

Fig. 12. Yaw error scenario 3.

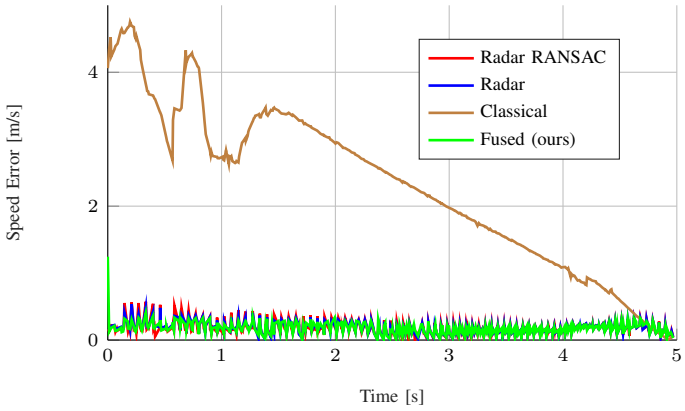

Fig. 13. Speed error scenario 3.

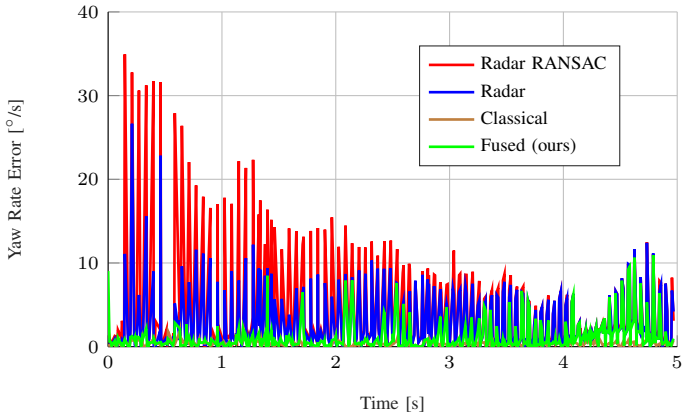

Fig. 14. Yaw rate error scenario 3.

and the integrated yaw. The trajectory of the fused result is qualitatively very close to the correct one. Interestingly, the radar odometry initially outperforms the classical one, whereas the classical odometry outperforms in the second half of the scenario.

2) Scenario 2: The estimation errors are presented in Fig. 7 - Fig. 10. Mean errors are summarized in Tab. IV. The classical odometry clearly has problems with the velocity estimation due to wheel slippage. As a result, position estimates are poor, too. On the other hand, the radar odometry has a problem with the yaw estimates. Two factors contribute to this fact. First, there is a higher amount of clutter in the snowy environment. We have even observed that the rear radars have more clutter measurements than the front ones, which might be due to the fact that the tires kick up snow. To some degree, the clutter can be suppressed by the static point selection featured in Sec. IV-B, however this cannot completely compensate for the effect of clutter measurements. Second, the motion model which is used in the measurement generation of the radar odometry is not entirely correct, since the lack of traction causes oversteering which results in a slight lurching movement which does not conform with the motion model. The fused algorithm eliminates the speed errors in comparison to the classical odometry and manages to reduce the yaw rate errors in comparison to the radar odometry. As a result, it achieves the best position estimates and comes close to the quality of the yaw estimates that can be obtained in the classical algorithm.

3) Scenario 3: The estimation errors are presented in Fig. 11 - Fig. 14. Mean errors are summarized in Tab. V. This experiment confirms the findings from the previous scenario. The classical algorithm has problems with the speed estimate due to blocked wheels. We see the problems due to clutter and model mismatch in the yaw rate estimate of the radar odometry again. The fused algorithm manages to reduce the yaw rate errors compared to the radar odometry estimates, whereas it maintains the low error in the speed estimate.

TABLE III
RESULTS SCENARIO 1

RMSE	***Position***	***Yaw***	***Speed***	***Yaw rate***
Radar RANSAC	8.22 m	8.1°	0.10 m/s	5.6 °/s
Radar	3.25 m	3.4°	0.05 m/s	2.1 °/s
Classical	1.75 m	1.2°	0.07 m/s	0.9 °/s
Fused (ours)	0.49 m	0.4°	0.05 m/s	0.9 °/s

TABLE IV
RESULTS SCENARIO 2

RMSE	***Position***	***Yaw***	***Speed***	***Yaw rate***
Radar RANSAC	0.61 m	4.4°	0.21 m/s	5.7 °/s
Radar	0.54 m	2.9°	0.21 m/s	3.4 °/s
Classical	25.29 m	0.1°	12.11 m/s	0.6 °/s
Fused (ours)	0.29 m	1.2°	0.15 m/s	2.3 °/s

TABLE V
RESULTS SCENARIO 3

RMSE	***Position***	***Yaw***	***Speed***	***Yaw rate***
Radar RANSAC	1.64 m	13.7°	0.19 m/s	6.6 °/s
Radar	0.87 m	7.9°	0.20 m/s	4.1 °/s
Classical	8.58 m	0.1°	2.52 m/s	0.5 °/s
Fused (ours)	0.39 m	1.8°	0.20 m/s	2.0 °/s

VI. CONCLUSION

We presented an approach that fuses radar measurements with wheel speed and gyrometer measurements. To this end, we detected the correctness of the sensors' outputs automatically based on the likelihood of the measurements with respect to the expected measurements. With this knowledge, the measurements were fused in a probabilistic manner. The result proved more more accurate than the combination of wheel speed and gyrometer measurements, under both adverse and good weather conditions in real world experiments. The fused estimate is more accurate than using only radar measurements. In addition, we validated our approach of using expected measurements for the static object measurement detection in the radar odometry pipeline rather than the RANSAC algorithm.

VII. Future Work

In future work, the initialization process could be investigated further to better handle the case when the vehicle is already moving when we start the algorithm. A link to simultaneous localization and mapping (SLAM) could be established based on the fact that both algorithms rely on static object detection. Position and orientation could be estimated in three dimensions based on the radar elevation measurements. More measurement modalities such as camera or lidar could be fused. Under adverse driving conditions, a different motion model could be used in order to describe the vehicle model more accurately.

ACKNOWLEDGMENT

The authors gratefully acknowledge funding by the Federal Office of Bundeswehr Equipment, Information Technology and In-Service Support (BAAINBw).

References

[1] M. Michaelis, P. Berthold, T. Luettel, and H.-J. Wuensche, "Generating Odometry Measurements from Automotive Radar Doppler Measurements," in *IEEE Symp. Sensor Data Fusion and Int. Conf. on Multisensor Fusion and Integration (SDF-MFI)*, 2023.

[2] N. J. Abu-Alrub and N. A. Rawashdeh, "Radar Odometry for Autonomous Ground Vehicles: A Survey of Methods and Datasets," *IEEE Trans. Intell. Veh.*, 2023.

[3] M. Mostafa, S. Zahran, A. Moussa, N. El-Sheimy, and A. Sesay, "Radar and Visual Odometry Integrated System Aided Navigation for UAVS in GNSS Denied Environment," *Sensors*, vol. 18, no. 9, 2018. [Online]. Available: https://www.mdpi.com/1424-8220/18/9/2776

[4] C. Doer and G. F. Trommer, "Radar visual inertial odometry and radar thermal inertial odometry: Robust navigation even in challenging visual conditions," in *Proc. IEEE/RSJ Int. Conf. Intelligent Robots and Syst. (IROS)*, 2021, pp. 331–338.

[5] A. Kramer, C. Stahoviak, A. Santamaria-Navarro, A.-a. Aghamohammadi, and C. Heckman, "Radar-Inertial Ego-Velocity Estimation for Visually Degraded Environments," in *Proc. IEEE Int. Conf. Robotics and Automation (ICRA)*, 2020, pp. 5739–5746.

[6] C. Doer and G. F. Trommer, "An EKF based approach to radar inertial odometry," in *Proc. IEEE Int. Conf. Multisensor Fusion and Integration (MFI)*, 2020, pp. 152–159.

[7] ——, "Radar inertial odometry with online calibration," in *European Navigation Conf. (ENC)*, 2020.

[8] Y. Z. Ng, B. Choi, R. Tan, and L. Heng, "Continuous-time radar-inertial odometry for automotive radars," in *Proc. IEEE/RSJ Int. Conf. Intelligent Robots and Syst. (IROS)*, 2021, pp. 323–330.

[9] M. Holder, S. Hellwig, and H. Winner, "Real-Time Pose Graph SLAM based on Radar," in *Proc. IEEE Intelligent Vehicles Symp. (IV)*, 2019, pp. 1145–1151.

[10] Y. Liang, S. Müller, D. Schwendner, D. Rolle, D. Ganesch, and I. Schaffer, "A Scalable Framework for Robust Vehicle State Estimation with a Fusion of a Low-Cost IMU, the GNSS, Radar, a Camera and Lidar," in *Proc. IEEE/RSJ Int. Conf. Intelligent Robots and Syst. (IROS)*, 2020, pp. 1661–1668.

[11] C. Kollberg, "Radar-Based Two-Dimensional Ego-Motion Estimation for Heavy Duty Vehicles," Master's thesis, KTH ROYAL INSTITUTE OF TECHNOLOGY, 2016.

[12] M. Sigonius, "Speed and yaw rate estimation in autonomous vehicles using Doppler radar measurements," Master's thesis, KTH ROYAL INSTITUTE OF TECHNOLOGY, 2018.

[13] D. Kellner, M. Barjenbruch, J. Klappstein, J. Dickmann, and K. Dietmayer, "Instantaneous ego-motion estimation using Doppler radar," in *Proc. IEEE Intelligent Transportation Syst. Conf. (ITSC)*, 2013, pp. 869–874.

[14] ——, "Instantaneous ego-motion estimation using multiple Doppler radars," in *Proc. IEEE Int. Conf. Robotics and Automation (ICRA)*, 2014, pp. 1592–1597.

[15] K. Thormann and M. Baum, "Single-frame radar odometry incorporating bearing uncertainty," in *IEEE Symp. Sensor Data Fusion and Int. Conf. on Multisensor Fusion and Integration (SDF-MFI)*, 2023.

[16] R. Huang, K. Zhu, S. Chen, T. Xiao, M. Yang, and N. Zheng, "A high-precision and robust odometry based on sparse MMW radar data and a large-range and long-distance radar positioning data set," in *Proc. IEEE Intelligent Transportation Syst. Conf. (ITSC)*, 2021, pp. 98–105.

[17] P.-C. Kung, C.-C. Wang, and W.-C. Lin, "A normal distribution transform-based radar odometry designed for scanning and automotive radars," in *Proc. IEEE Int. Conf. Robotics and Automation (ICRA)*, 2021, pp. 14 417–14 423.

[18] C. H. Schiller, B. Arsenali, D. Maas, and S. Maranó, "Improving marine radar odometry by modeling radar resolution and exploiting additional temporal information," in *Proc. IEEE/RSJ Int. Conf. Intelligent Robots and Syst. (IROS)*, 2022, pp. 8436–8441.

[19] R. Zhang, Y. Zhang, D. Fu, and K. Liu, "Scan denoising and normal distribution transform for accurate radar odometry and positioning," *IEEE Robot. Autom. Lett.*, vol. 8, no. 3, pp. 1199–1206, 2023.

[20] Y. Zhuang, B. Wang, J. Huai, and M. Li, "4D iRIOM: 4D Imaging Radar Inertial Odometry and Mapping," *IEEE Robot. Autom. Lett.*, vol. 8, no. 6, pp. 3246–3253, 2023.

[21] S. H. Cen and P. Newman, "Precise Ego-Motion Estimation with Millimeter-Wave Radar Under Diverse and Challenging Conditions," in *Proc. IEEE Int. Conf. Robotics and Automation (ICRA)*, 2018, pp. 6045–6052.

[22] ——, "Radar-only ego-motion estimation in difficult settings via graph matching," in *Proc. IEEE Int. Conf. Robotics and Automation (ICRA)*, 2019, pp. 298–304.

[23] H. D. Flemmen, R. Mester, A. Stahl, T. H. Bryne, and E. F. Brekke, "Maritime radar odometry inspired by visual odometry," in *Proc. Int. Conf. Information Fusion (FUSION)*, 2023, pp. 1–8.

[24] M. Barjenbruch, D. Kellner, J. Klappstein, J. Dickmann, and K. Dietmayer, "Joint spatial- and Doppler-based ego-motion estimation for automotive radars," in *Proc. IEEE Intelligent Vehicles Symp. (IV)*, 2015, pp. 839–844.

[25] J. Michalczyk, R. Jung, and S. Weiss, "Tightly-coupled EKF-based radar-inertial odometry," in *Proc. IEEE/RSJ Int. Conf. Intelligent Robots and Syst. (IROS)*, 2022, pp. 12 336–12 343.

[26] J. Michalczyk, R. Jung, C. Brommer, and S. Weiss, "Multi-state tightly-coupled EKF-based radar-inertial odometry with persistent landmarks," in *Proc. IEEE Int. Conf. Robotics and Automation (ICRA)*, 2023, pp. 4011–4017.

[27] K. Burnett, D. Yoon, A. Schoellig, and T. Barfoot, "Radar odometry combining probabilistic estimation and unsupervised feature learning," in *Proc. Int. Conf. Robotics: Science and Syst. (RSS)*, 2021.

[28] P. Berthold, M. Michaelis, T. Luettel, D. Meissner, and H.-J. Wuensche, "A Radar Measurement Model for Extended Object Tracking in Dynamic Scenarios," in *Proc. IEEE Intelligent Vehicles Symp. (IV)*, 2019, pp. 770–776.

[29] ——, "Probabilistic Vehicle Tracking with Sparse Radar Detection Measurements," *ISIF Journal of Advances in Information Fusion*, vol. 17, no. 2, pp. 116–139, 2022.